Paper No.
648

CORROSION 98

GALVANIC INTERACTION BETWEEN CARBON FIBER REINFORCED PLASTIC (CFRP) COMPOSITES AND STEEL IN CHLORIDE CONTAMINATED CONCRETE

Andrés A. Torres-Acosta*, Alberto A. Sagüés, and Rajan Sen.
Department of Civil and Environmental Engineering.
University of South Florida
4202 E. Fowler Ave.
Tampa, FL 33620.

ABSTRACT

Experiments were performed to determine the possible extent of galvanic corrosion when CFRP and steel are in contact in chloride contaminated concrete. Three concrete environments (water-to-cement (w/c) ratio of 0.41) at relative humidities (R.H.) of ~60%, ~80% and ~95%, and 14 kg/m^3 chloride were investigated. The CFRP composite potential reached between -180 and -590 mV (vs CSE) when it was in contact with steel at these environments. Results showed significant galvanic action in the 80% RH chloride contaminated concrete (nominal steel current densities as high as 0.3 μA/cm^2).

Keywords: galvanic corrosion, CFRP, Carbon Fiber Reinforced Plastics, concrete, relative humidity, chloride contamination.

INTRODUCTION

Pore water in concrete is alkaline typically with pH between 12.5 and 13.7.[1-2] This range of pH results in a low corrosion rate for steel because of passivity of the metal surface. The passive film acts as a barrier that protects the steel against further corrosion. However, this barrier may be disrupted by external agents like chloride ions that reach the rebar depth by penetration from the external environment. The ensuing corrosion causes significant damage.[3]

Fiber reinforced plastics (FRP's) are potential alternative candidates to steel for reinforcing concrete. FRP's have high strength to weight ratio, and many of them provide excellent resistance to corrosion. CFRP is a lightweight, high strength, high modulus FRP with exceptional resistance to fatigue and chemical attack.

*Permanent Affiliation CINVESTAV.IPN, Mérida, Yucatán, México.

CFRP is increasingly being used world wide in numerous bridge structures including one in Calgary that was opened to traffic in 1993.[4] Since CFRP is relatively brittle, some steel may still be required for stirrups or for secondary prestressing reinforcement. Unlike aramid or glass,[5] carbon fibers are conductors of electricity and can support electrochemical reactions. When carbon and steel are coupled in an electrolyte, such as wet concrete, galvanic corrosion may take place with steel as the anode and carbon as the cathode.[6] The effect could occur even with epoxy coated steel at breaks in the coating.

Several investigations of the galvanic interaction of CFRP and metals in chloride contaminated solutions have been conducted recently.[7-10] However, the galvanic effect in concrete has received little attention.[11] This work intends to further evaluate the extent of galvanic action arising from direct contact between CFRP and steel in chloride contaminated concrete.

REINFORCING MATERIALS PROPERTIES

CFRP Specimens

The CFRP composite used was a rod shaped pultruded carbon fiber composite ~6 mm diameter. This rod was supplied as a 50,000 filament continuous tow by AKZO Industries, and is made from FORTAFIL® 3(C) continuous carbon fiber (~ 7 μm diameter). The fiber volume was approximately 53 %. The external surface of the rod was covered with a sand grit composite to enhance bond with concrete. Figure 1 shows optical micrographs of longitudinal and transversely cross sections in the as received condition. The mechanical properties of the composite are summarized in Table 1.[12]

Steel Specimens

Steel used in this experiment was plain wire 5.5 mm in diameter (ASTM A 82) commonly used for spiral reinforcement in concrete. Metallographic examination revealed a ferritic microstructure with low carbon (< 0.1 %) content. The wire surface was sandblasted and degreased with acetone prior to casting in concrete.

EXPERIMENTAL PROCEDURE

Sample Preparation

Eighteen reinforced concrete prisms 5 x 10 x 19 cm were used as galvanic cells (See Table 2 for mix design). All the prisms were contaminated with chlorides by adding 3% NaCl by weight of cement at the time of mixing. Two CFRP specimens and one steel specimen were cast in each cell. Each rod (CFRP or steel) had a 19 cm length (32 cm^2) in contact with the concrete. Figure 2 shows the cell configuration. Both ends of the steel wire were cast in a 2.5 cm diameter, 2.5 cm long chloride free mortar plug (w/c = 0.5) to avoid corrosion at the exit points. Furthermore, the steel and the mortar at the exit points were sealed with epoxy. The plugs were allowed to cure for 7 days before placement in the prism mold.

The CFRP specimens used in this experiment were tested in the following conditions: SI, with the side surface in the initial, as-received condition; SD01, with side surface mechanically degraded by filing off 0.1% of the surface layer of the CFRP composite, and SD10 with 1% of the surface layer removed. The filing marks were typically 1 mm wide, 2 mm long and 0.5 mm deep, uniformly spaced and in sufficient numbers

to reach the percentage damage specified. These surface conditions were examined to determine the difference in electrochemical action of as-received surface with grit composite vs damaged grit composite and exposed fibers. Mechanical damage at the lateral surface may happen in actual construction practice, during handling, placing and casting of the composite in concrete structural members.

Individual electrical connections of both steel and CFRP specimens were made to external wiring. CFRP contact resistances of $< 1\Omega$ were achieved with 9 mm long galvanized or stainless steel screws placed inside a drilled-and-tapped hole in one of the CFRP ends. A copper cable was attached to the screw. After placing 5 mm of the screw inside the CFRP, a carbon conductive paint film was applied to the connection, to ensure electrical continuity of the entire CFRP composite. An epoxy coating encased the connection to avoid possible moisture-induced external galvanic effects.

The experiments (all at 22±2°C) involved six consecutive stages:

a. A curing stage in which the concrete prisms were cast and wet cured for 30 days (the CFRP and steel specimens were not interconnected).
b. A stabilization stage, in which the prisms were then divided into groups and placed in three different R.H. chambers (~95 % R.H., ~80 % R.H., and ~60 % R.H.). The duration of this stage was approximately 40 days.
c. First coupling stage, where the prisms remained in their respective chambers and one CFRP rod was electrically connected with the steel rod in each prism, for a period of 80 days. In this stage the CFRP/steel surface area ratio was 1:1.
d. A first uncoupling stage, from day 150 trough day 200, in which CFRP and steel were disconnected and allowed to depolarize.
e. A second coupling stage (from day 200 through day 425) in which the two CFRP specimens in each concrete prism were connected to the steel. The CFRP/steel surface area ratio in this stage was 2:1.
f. A final uncoupling stage, in which the galvanic couples were permanently disconnected for future investigation.

Potential and Galvanic Current Measurements

Potential measurements were periodically made using a 200 MΩ impedance DC voltmeter. They were measured versus a copper-copper sulfate electrode (CSE) with the sensing tip placed on the top surface of the concrete prism. During the coupling stages (c) and (e), the potentials of the CFRP and steel specimens were measured in the "instant-off" condition to avoid errors due to ohmic potential drop in the electrolyte. A CMS100 Corrosion Measurement System from Gamry Instruments, Inc., configured as a zero resistance ammeter (ZRA) was used to measure the galvanic currents between the CFRP and steel specimens during coupling stages (c) and (e).

Cyclic Polarization Tests

During stage (e), cyclic polarization tests were performed to qualitatively evaluate the ability of the CFRP to act as a cathode at potentials as low as -700 mV vs CSE. These experiments were made with a CMS100 from Gamry Instruments Inc. with a Potentiostat/Galvanostat/ZRA.

The experiment started with a forward scan rate of 0.1 mV/sec. towards cathodic potentials. The potential of the sample was swept from the open circuit potential (E_{OC}), to the apex potential (defined as 500 mV more negative than E_{OC}), where the scan direction was reversed. The reverse scan rate was also 0.1 mV/sec. The sampling period, or spacing between data points, was chosen to be 10 sec. The experiments were performed

using the steel rod as the counter electrode, one of the CFRP rods as the reference electrode, and the other CFRP rod in the concrete prism as the working electrode. The scan rate used was chosen based on previous experiments done with the same CFRP composite in saturated calcium hydroxide ($Ca(OH)_2$) solutions and mortars.[13] From those results it was concluded that scan rate effects where not overwhelming at rates < 0.25 mV/sec.

The test results were IR compensated by subtracting the product of the effective concrete resistance[14] (measured at ~ 100 Hz using the three-electrode configuration) and the applied current, from the potential measured at the reference electrode.

RESULTS AND DISCUSSION

Figures 3-5 show the potentials and galvanic currents (average of two specimens) as a function of time for each of the three R.H. environments. The vertical lines delimit the consecutive exposure stages (a) through (f) as indicated above each graph. The following observations and comments apply:

Curing, Stabilization and Uncoupled Stages

CFRP potentials before galvanic coupling with steel were typically -200 mV ±100 mV CSE for all surface conditions and R.H. regimes. Somewhat more positive potentials were observed during the later stages of uncoupling (d,f).

Steel potentials were quite negative (≈-600 mV CSE) during the curing stage and ≈-350 mV CSE average in the stabilization stage. In the later uncoupled periods steel potentials increased to more positive values but still typically 100 mV to 200 mV more negative than those of the CFRP. The potential values (and spontaneous fluctuations) in all three humidity regimes were characteristic of actively corroding steel,[15] as expected from the high chloride ion content of the concrete.

Coupling Stages

In all cases, the steel acted as the anode in the galvanic couple. The galvanic currents spanned a wide range, from the instrument detection limit (< 0.1 nA) up to 10 μA. Considerable galvanic current fluctuation existed as a function of time, especially in the 80% and 60% R.H. regimes. When coupled, the potentials of both steel and CFRP were quite close, appeared to continue the trend of the steel during the uncoupled stages, and were more negative than those of the CFRP during the uncoupled stages.

The combined graphs of Figures 6-8 were made by cross-plotting the individual potential and galvanic current values from each specimen history, during stage c (open rectangles) and stage e (open triangles), in the manner of a polarization diagram. The results indicate a correlation between the spontaneous variations in the steel-composite potential and the observed galvanic currents (higher currents when the potential is more negative). These observations, plus those mentioned earlier, strongly suggest that the steel dominated the potential of the galvanic couple.

The highest galvanic current values (10 μA) observed were for the 80% R.H. environment during stage (e), when the steel potential experienced potential excursions approaching -500 mV CSE (see Figure 7). The highest galvanic currents for the 95% R.H. environments (Stage (c)) was < 1 μA, even though the potential reached almost -600 mV CSE (see Figure 6). The highest currents were below 1.5 μA in the 60% R.H. tests

(see Figure 8), for which the potential tended not to be as negative as in the other environments (>-450 mV CSE). The magnitude of the galvanic currents may be expected to be greater during stage "e" (2:1 CFRP/steel area ratio) than during stage "c" (1:1 ratio). A few results (for example for 80% R.H. at potentials ≤-400 mV, Figure 7) appear to support that expectation, but the overall data set could not clearly differentiate between both area ratio regimes.

Cyclic Polarization

The results of the CFRP cyclic polarization tests are superimposed on the combined polarization diagrams of Figures 6-8. For clarity, results for only one of a duplicate set of tests are shown; the duplicates yielded essentially the same conclusions. There was no consistent differentiation between the results for different surface conditions. Relatively little hysteresis is apparent in the 95% and 80% R.H. tests. For all the environments, the cathodic currents obtained in the cyclic polarization tests are comparable to those from the combined long term behavior at the same potentials.

The tests at 95% R.H. show an apparent limiting current behavior at ≈ 1-10 μA, whereas at 80% R.H. the limitation (if any) develops at much higher currents. The polarization behavior suggests that the galvanic current corresponded to a cathodic reaction on the CFRP surface, which in concrete is likely to result from oxygen reduction.[15-16] This interpretation would agree with limiting current behavior at 95% R.H. (since low oxygen diffusivity is expected in nearly water-saturated concrete[17]), and mostly activation-limited polarization at 80% R.H. when oxygen diffusivity should be higher. The results from the tests at 60% R.H., while less conclusive because of pronounced hysteresis, seem to further support that view.

Based on the above discussion, the magnitude of the galvanic currents seems to respond to the corrosion potential of the steel and be limited by the oxygen reduction reaction at the CFRP surface. Maximum currents developed at 80% R.H. At higher and lower humidities the extent of the galvanic current appeared to have been limited by oxygen transport and by the corrosion condition of the steel respectively. The worst case currents (10μA) corresponded to a nominal galvanic current density of 0.3 $\mu A/cm^2$ on the steel surface. This level of anodic galvanic current density can be a significant corrosion aggravating factor, since comparable corrosion current densities can cause cracking of the concrete cover in a few years: corrosion rates on the order of 0.5 $\mu A/cm^2$ may produce visible cracks at the concrete surface (for concrete covers ≤ 30 mm) in about 5 to 10 years.[18]

Implications and additional issues

As indicated in the introduction, engineering constraints may require the use of metallic stirrups with CFRP tendons, at least during the initial applications of this new material. Structural design for CFRP prestressed beams may be expected to require a CFRP/stirrup steel area ratio on the order of 10:1.[4] The concrete resistivity and beam geometry may limit the mutual throwing power of the galvanic system, so that the effective area ratio could be less. However, as shown above significant steel corrosion aggravation can develop with moderate area ratios. For epoxy-coated steel stirrups galvanic corrosion would not be an issue as long as complete electric insulation between CFRP and the steel were achieved. However, accidental contact may occur through abrasion or tie wire damage at joints.[19] Such contact could result in large CFRP/exposed steel area ratios at small coating breaks elsewhere in the stirrup, with potentially severe consequences. The extent of these possible effects merits further investigation.

The effect of the galvanic currents on the integrity of the CFRP itself was not addressed here, but should be considered in future work. Previous studies [7-10,20] have shown disbondment between the epoxy matrix and

the carbon fibers when the CFRP is cathodically polarized in chloride contaminated solutions. A subsequent phase of this investigation is examining the extent of those effects in concrete.

CONCLUSIONS

1. Galvanic coupling between CFRP and steel in chloride contaminated concrete produced anodic currents on the steel. The galvanic current was greatest at intermediate R.H. levels. The highest nominal steel current densities were 0.3 $\mu A/cm^2$, when the concrete was exposed to an 80% R.H. environment with a CFRP:steel area ratio of 2:1.

2. The steel dominated the potential of the galvanic couple. The cathodic current on the CFRP was interpreted as corresponding to oxygen reduction, showing signs of concentration polarization at 95% R.H. and potentials more negative than -400 mV CSE.

ACKNOWLEDGMENTS

The authors are indebted to the University of South Florida for partial support of this investigation. The opinions and findings in this paper are those of the authors and not necessarily those of the funding agencies. One of the authors (A.A.T.A) acknowledges the scholarship provided by the National Council of Science and Technology (CONACYT-México).

REFERENCES

1. K.K. Sagoe-Crentsil and F.P. Glasser, *Mag. Conc. Res.*, 41, 149(1989): p. 205.
2. R.S. Barneyback and S. Diamond, *Cem. and Conc. Res.*, 11, 2(1981): p. 279.
3. C.D. Newhouse and R.E. Weyers, *Techniques to Assess the Corrosion Activity of Steel Reinforced Concrete Structures*, STP 1276, (Philadelphia, PA: ASTM, 1996), p. 3.
4. S.H. Rizkalla and G. Tadros, *Concrete International*, 16, 6(1994): p. 42.
5. P.K. Mallick, *Fiber-Reinforced Composites: Materials, Manufacturing and Design* (New York, NY: Marcel Dekker, Inc., 1988).
6. W.C. Tucker, R. Brown and L. Russell, *J. of Composite Mats.*, 24, (1990): p. 92.
7. D. Kaushik, M.N. Alias and R. Brown, *Corrosion*, 47, 11(1991): p. 859.
8. M.N. Alias and R. Brown, *Corrosion*, 48, 5(1992): p. 373.
9. D.M. Aylor, *High temperature and Environmental Effects on Polymeric Composites*, STP 1174 (Philadelphia PA: ASTM, 1993), p. 81.
10. S.R. Taylor, F.D. Wall and G.L. Cahen, *J. Electrochem. Soc.*, 143, 2(1996): p. 449.
11. A.A. Torres-Acosta, A.A. Sagüés and R. Sen, *Proceedings of the Second International Conference on Advanced Composite Materials in Bridges and Structures (*Montreal, Canada:ACMBS-II, 1996), p. 141.
12. AKZO, Technical Data Sheet 902A, Fortafil Fibers, Inc., Rockwood, TN 37854, 1994.
13. A.A. Torres-Acosta, "Polarization Behavior of Carbon Fiber-Reinforced Plastic Strands used in Prestressed Concrete," *IV International Conference on Advanced Materials*, invited paper, poster presentation, (Mexico City, Mexico, 1995).
14. S.G. Millard, *Proc. Instn. Civ. Engrs.*, Part 2, 91, Mar.(1991): p. 71.

15. A. Aguilar, A.A. Sagüés, and R.G. Powers, *Corrosion Rates of Steel in Concrete*, STP 1065, (Philadelphia, PA: ASTM, 1990), p. 66.
16. C. Andrade, C. Alonso and A.M. García , *Advances in Cem. Res.*, 3, 11(1990): p. 127.
17. O.E. Gjørv, O. Vennesland and A.H.S. El-Busaidy, *Mater. Perform.*, 25, 12(1986): p. 39.
18. C. Andrade, C. Alonso and F.J. Molina, *Mats. and Structs.*, 26, (1993), p. 453.
19. A.A. Sagüés, "Corrosion of Epoxy Coated Rebar in Florida Bridges," Final Report to Florida D.O.T., WPI No. 0510603, May, 1994 (Available from FDOT Research Center, Tallahassee, FL).
20. S.R. Taylor, *Comp. Interf.*, 2, 6(1994), p.403.

TABLE 1
Carbon Fiber and Composite Properties (from manufacturer specs).

Material Properties	Carbon Fiber	Composite
Tensile Strength	3,800 MPa	1,450 MPa
Tensile Modulus	227 GPa	121 GPa
Ultimate Elongation	1.7%	1.5%
Density	1.8 g/cm^3	
Cross Section Area	4.3x10-5 mm^2	29.7 mm^2
Filament Diameter	7.3 μm	
Axial Thermal Expansion	-0.1μm/m/°C	25 μm/m/°C

TABLE 2
Mix Proportions for Concrete Prisms.

Material	Content (kg/m^3)
Type I Portland Cement	391
Water	177
Fine Aggregate (Silica Sand)	776
Coarse Aggregate (Limestone, 1 cm max. size)	866
Calculated Total Cl^- Concentration	14

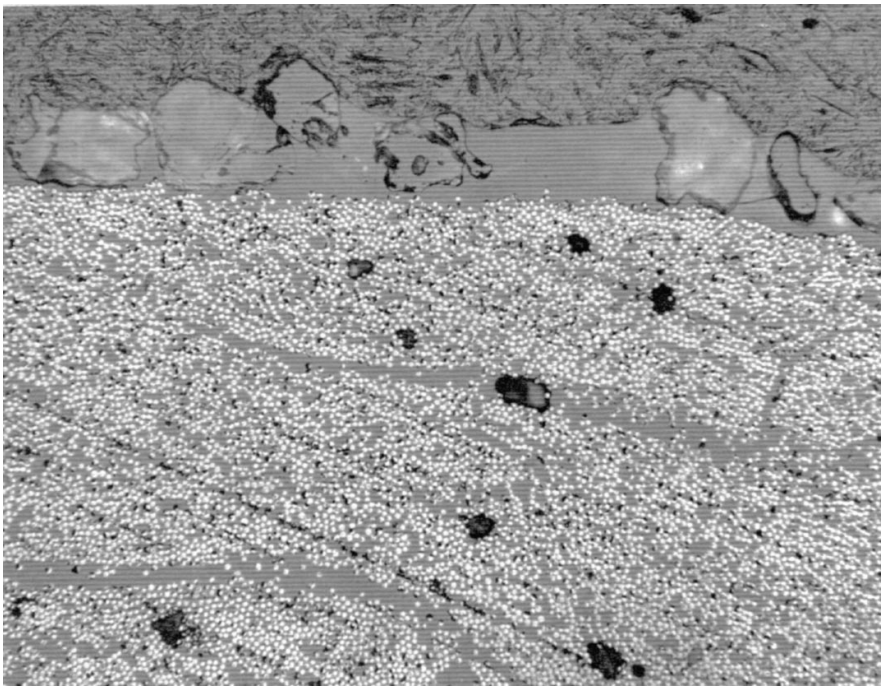

Figure 1. Optical micrographs of CFRP composite in the as received condition. Top, transverse cross section; bottom, longitudinal cross section.

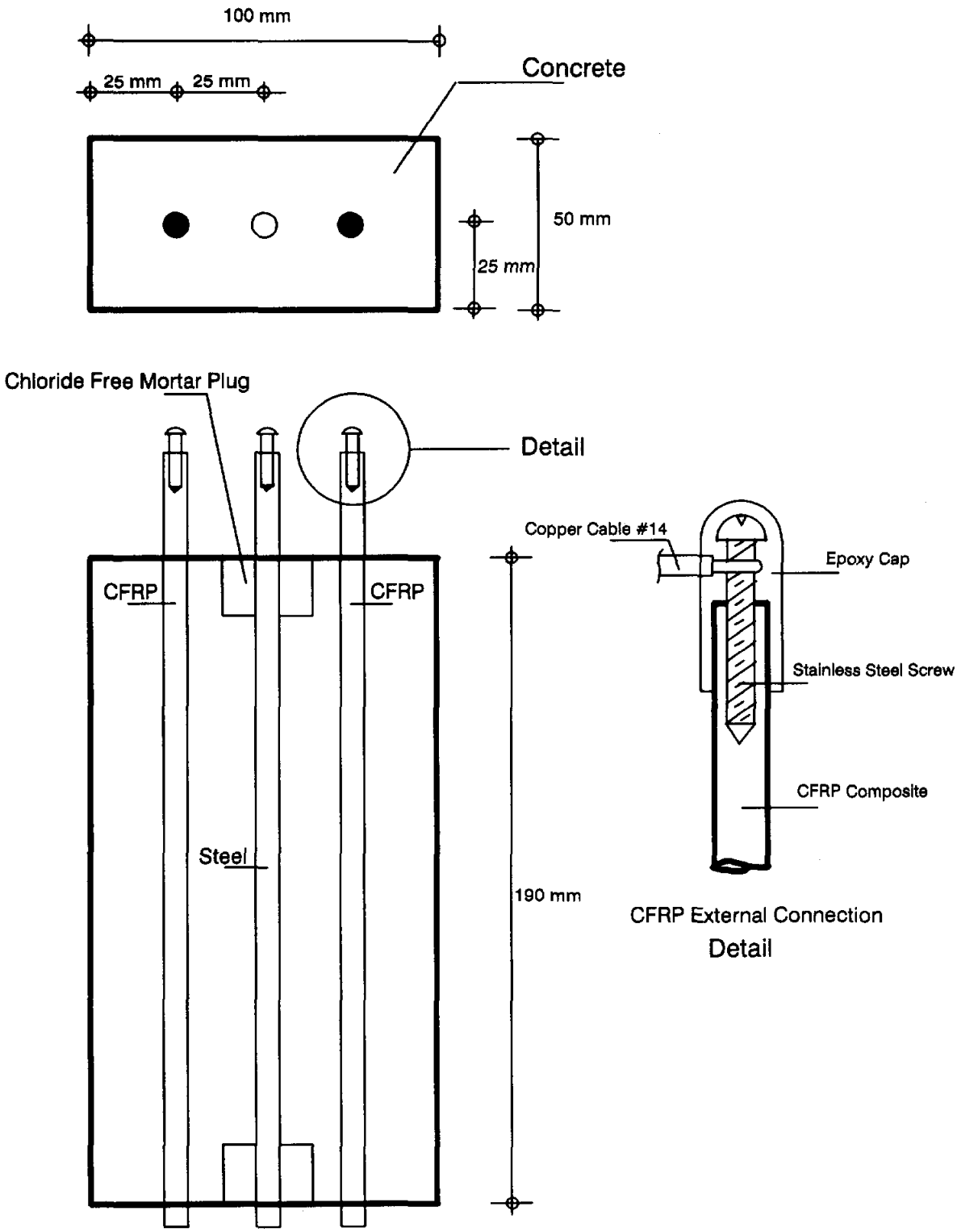

Figure 2. Concrete Galvanic Cell Geometry.

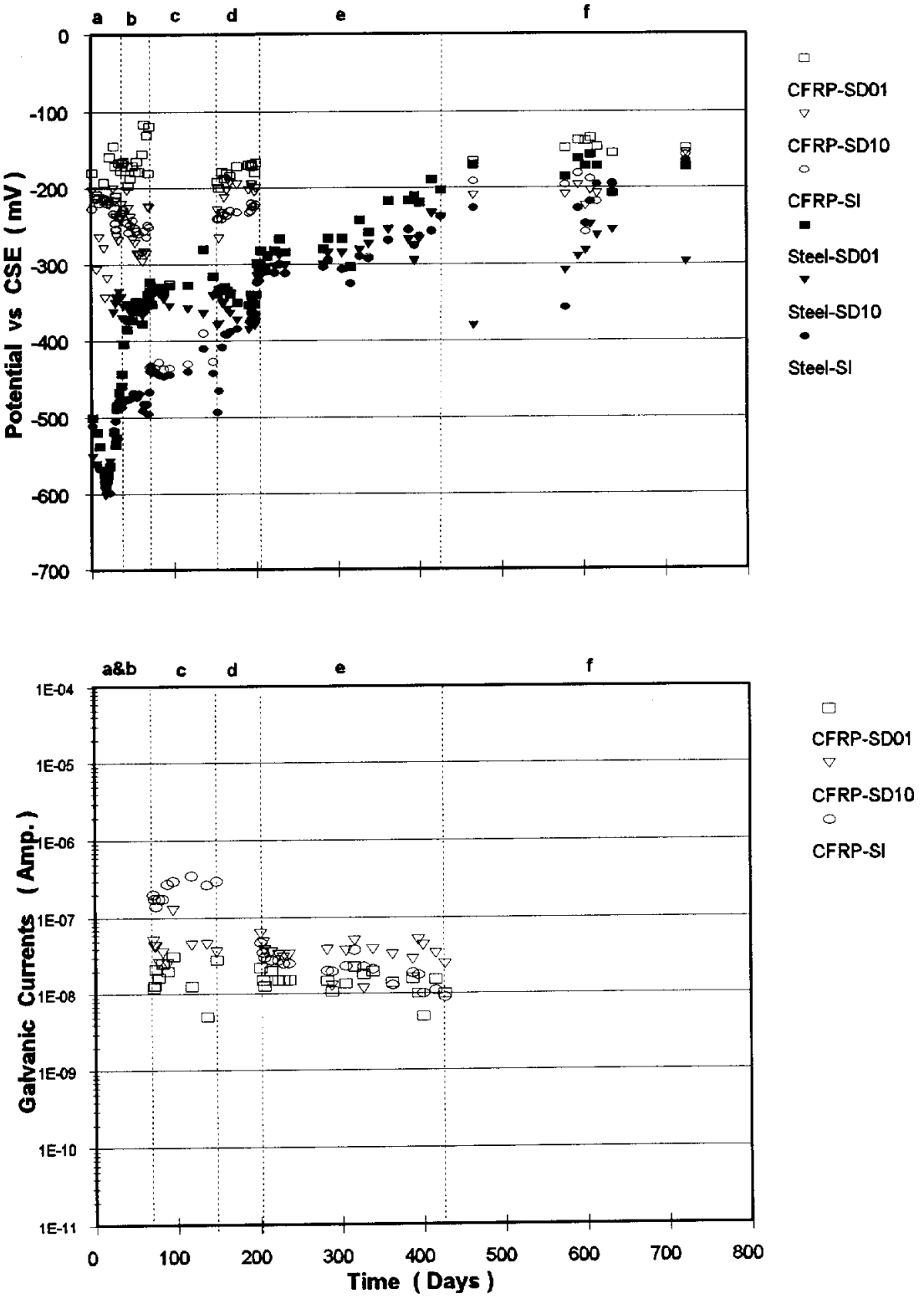

Figure 3. Average potential and galvanic current vs time at~ 95% R.H. in chloride-contaminated concrete. (a-f): experimental stages.

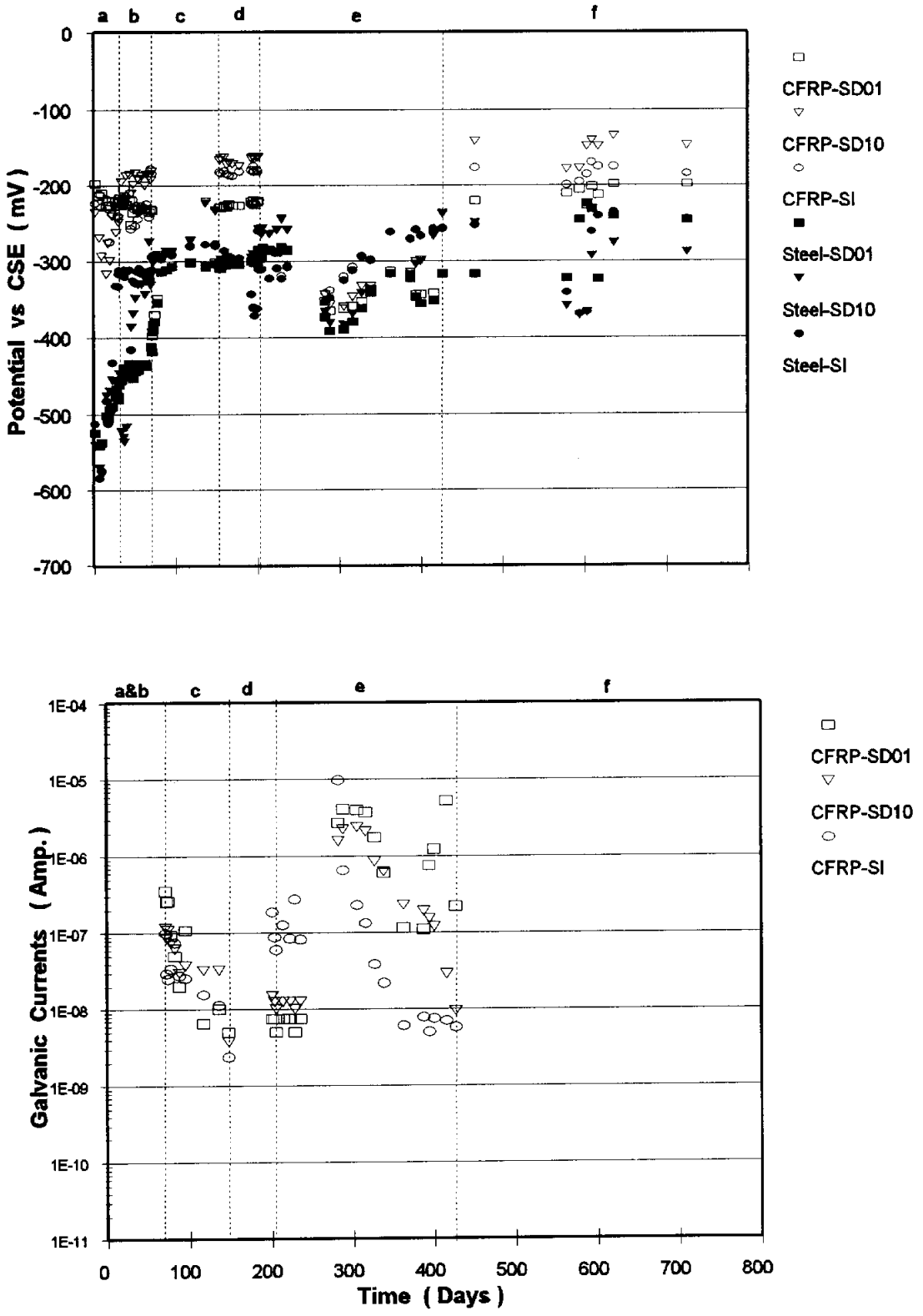

Figure 4. Average potential and galvanic current vs time at ~ 80% R.H. in chloride-contaminated concrete. (a-f): experimental stages.

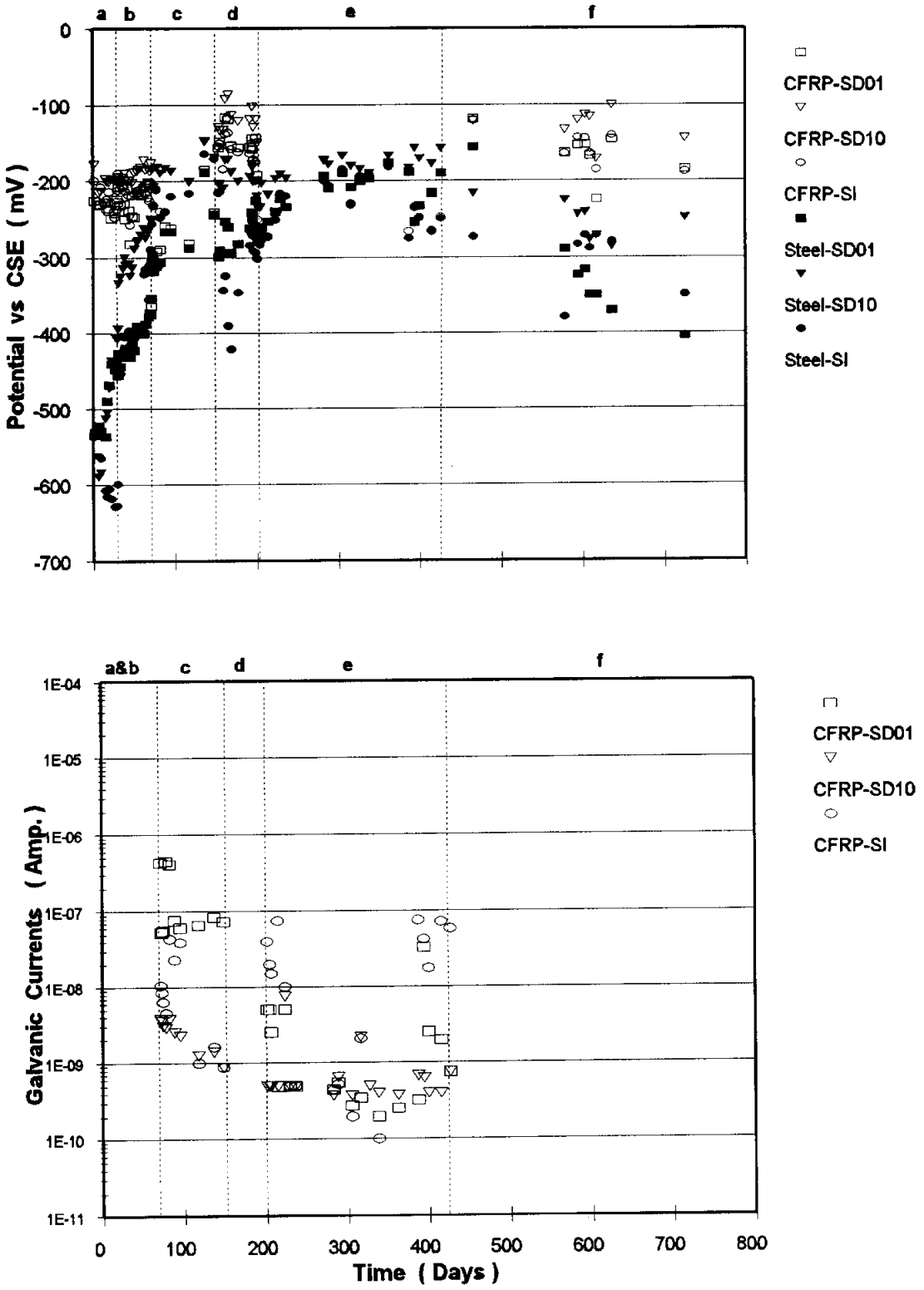

Figure 5. Average potential and galvanic current vs time at ~ 60% R.H. in chloride-contaminated concrete. (a-f): experimental stages.

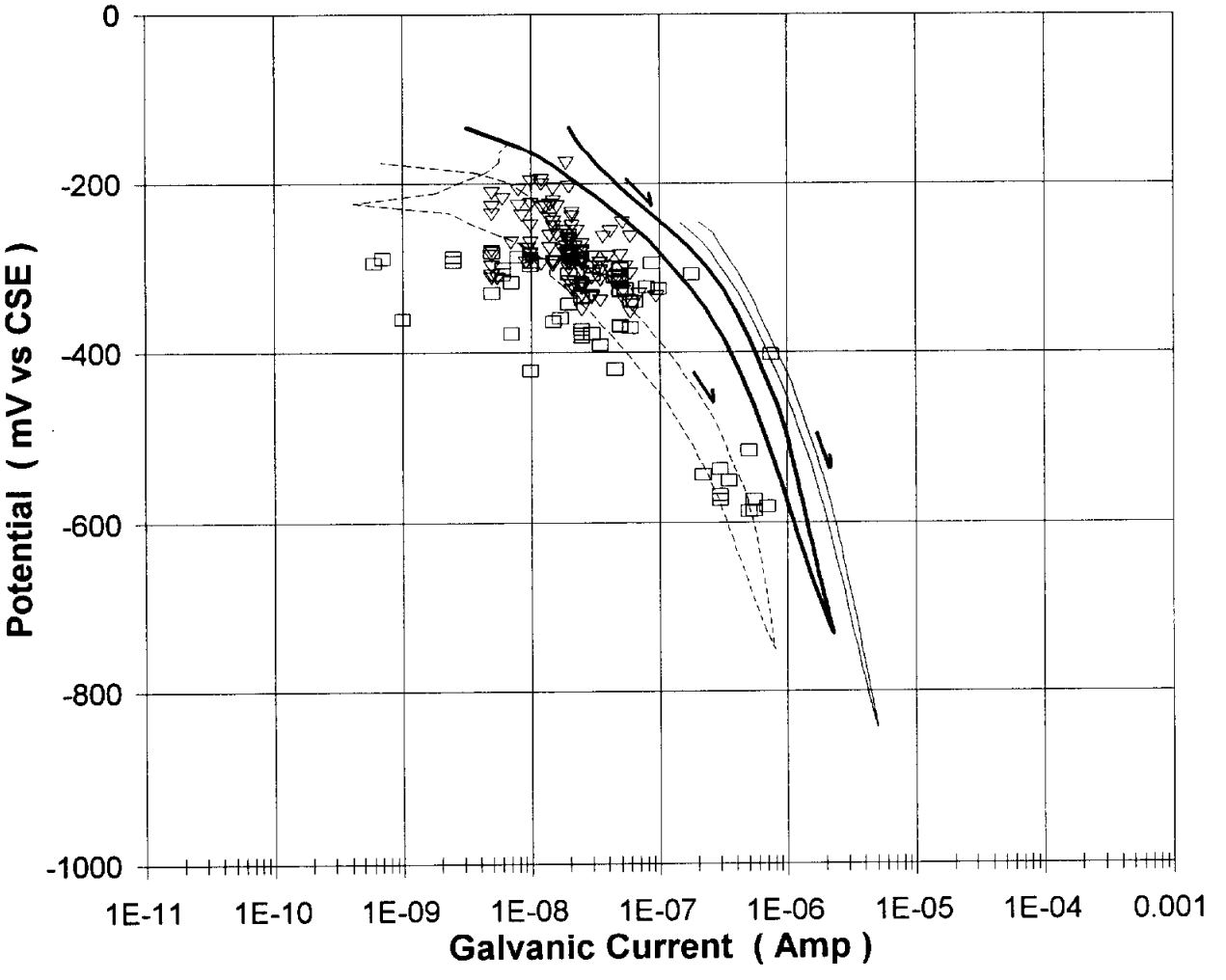

Figure 6. Combined CFRP potential-current plot for ~95% RH environment.
(□) Coupling stage "c" (1:1 CFRP:steel area ratio)
(▽) Coupling stage "e" (2:1 area ratio)

——— Cyclic polarization, as received
----- Cyclic polarization, 0.1 % surface damage
—— Cyclic polarization, 1 % surface damage

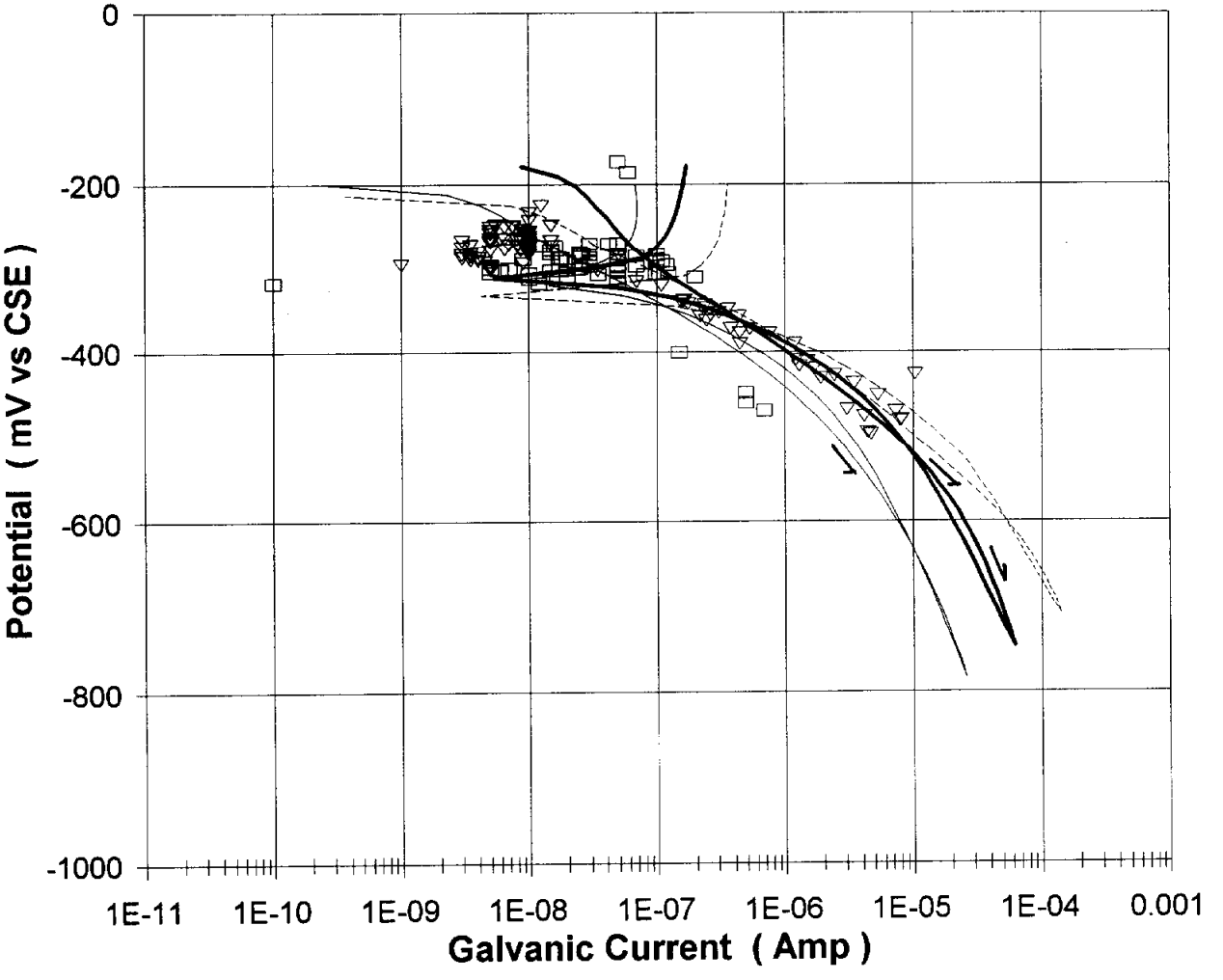

Figure 7. Combined CFRP potential-current plot for ~80% RH environment.
(□) Coupling stage "c" (1:1 CFRP:steel area ratio)
(▽) Coupling stage "e" (2:1 area ratio)

——— Cyclic polarization, as received
----- Cyclic polarization, 0.1 % surface damage
——— Cyclic polarization, 1 % surface damage

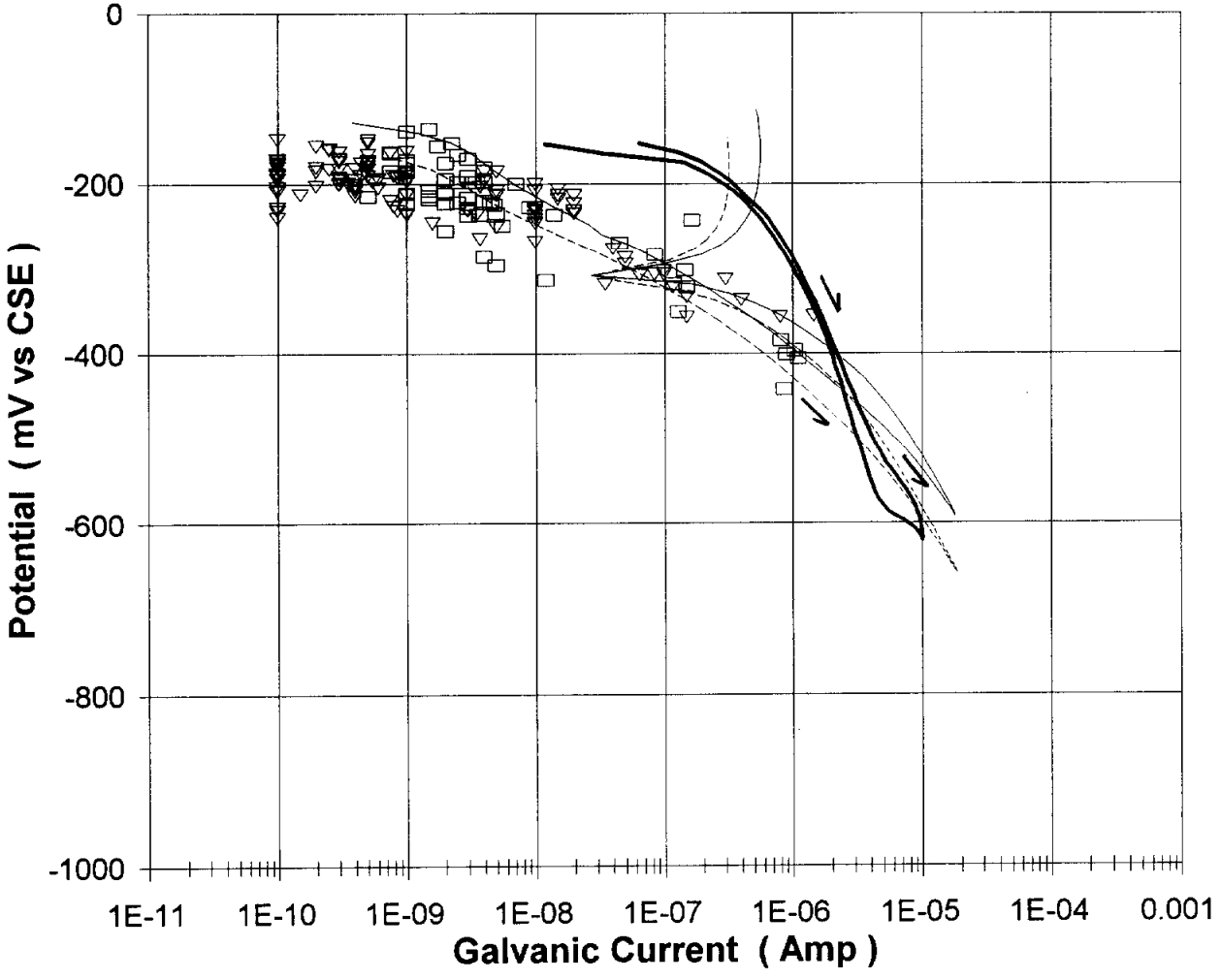

Figure 8. Combined CFRP potential-current plot for ~60% RH environment.
(□) Coupling stage "c" (1:1 CFRP:steel area ratio)
(▽) Coupling stage "e" (2:1 area ratio)

——— Cyclic polarization, as received
----- Cyclic polarization, 0.1 % surface damage
—— Cyclic polarization, 1 % surface damage